

RESEARCH

Open Access



# A self-adjuvant multiantigenic nanovaccines simultaneously activate the antiviral and antitumor immunity for the treatment of cancers

Zhongjie Wang<sup>1†</sup>, Hanlin Chen<sup>1†</sup>, Ruiqi Ming<sup>1</sup>, Weiwei Wang<sup>1</sup>, Shujun Liu<sup>1</sup>, Yuantian Jing<sup>1</sup>, Zewei Yan<sup>3</sup>, Guihong Lu<sup>2\*</sup> and Li-Li Huang<sup>1\*</sup>

## Abstract

**Background** Tumor cell-derived extracellular vesicles (tEVs) have garnered significant attention as promising antigen delivery vehicles for the development of cancer vaccines. However, their practical applications are hindered by weak immunogenicity and inadequate lymph node targeting. In this study, we engineered tEVs into “self-adjuvant” multiantigenic nanovaccines that simultaneously accumulate in tumors and lymph nodes (LNs), effectively triggering innate and adaptive immunity capable of recognizing both tumor cells and virus antigen-modified tumor cells to inhibit tumor progression.

**Results** 4T1 tumor cells were infected with vesicular stomatitis virus (VSV), leading to the expression of VSVG and calreticulin (CRT) on their surface. Using these infected cells, we prepared extracellular vesicles (vEVs) carrying both VSVG and CRT. When injected subcutaneously, vEVs targeted tumors effectively due to the homologous targeting capability of tumor cell membranes. In which, VSVG induced fusion between vEVs and tumor cells, creating viral antigen-decorated tumor cells, which enhanced the recognition and phagocytosis of tumor cells by macrophages. Additionally, the surface CRT of vEVs activated the “eat-me” signaling, thus improving their recognition and uptake by dendritic cells (DCs). This led to DC maturation and the activation of antiviral and antitumor T cells, synergistically inhibiting tumor growth.

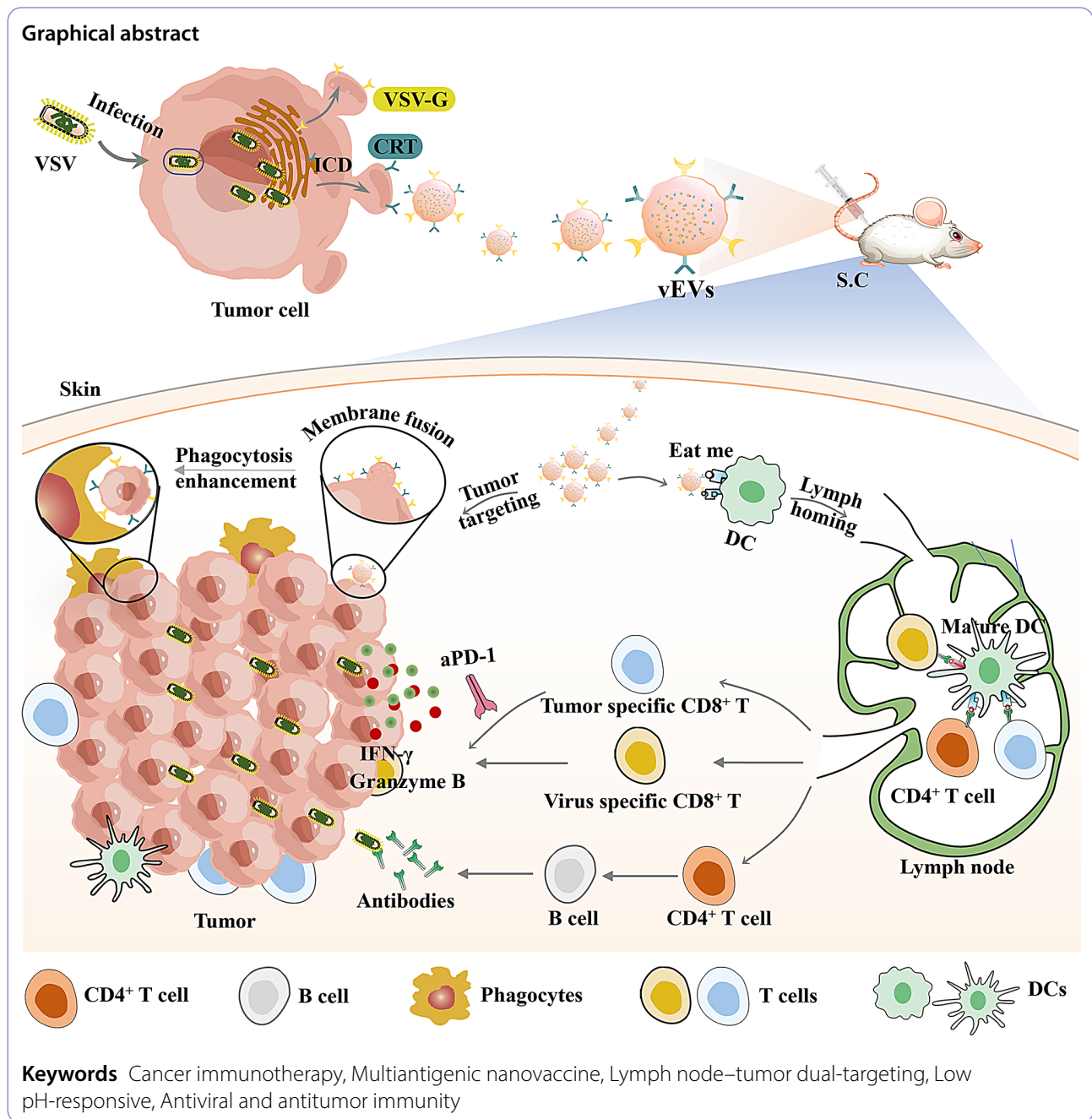
**Conclusions** This research introduces a straightforward yet efficacious methodology for the production of cancer vaccines to fight cancer through the stimulation of both the antiviral and antitumor immune responses within the body.

<sup>†</sup>Zhongjie Wang and Hanlin Chen co-first authors.

\*Correspondence:  
Guihong Lu  
lu\_guihong@163.com  
Li-Li Huang  
llhuang@bit.edu.cn

Full list of author information is available at the end of the article





## Background

Cancer vaccines represent a revolutionary approach in the field of cancer immunotherapy, holding immense potential in the battle against various types of cancer [1]. Cancer vaccination typically involves the administration of tumor antigens and adjuvants to activate the body's immune response, achieving the goal of inhibiting tumor cell growth, metastasis, and recurrence [2]. The design of tumor vaccines necessitates the careful selection and delivery of antigens and adjuvants to dendritic cells (DCs) via nanocarriers, ensuring precise recognition

and uptake, followed by the activation of the immune response through T lymphocyte antigen presentation [3].

Tumor cell-derived extracellular vesicles (tEVs) have emerged as promising vaccine candidates due to their ability to encapsulate a wide array of tumor antigens, including both tumor-specific antigens (TSAs) and tumor-associated antigens (TAAs) [4–6]. This broad antigen spectrum significantly reduces the risk of immune evasion compared to single-epitope vaccines and circumvents the need for the laborious and expensive process of antigen identification [7]. Additionally, the

biocompatibility and inherent tumor-targeting capabilities of tEVs make them exceptional carriers for anticancer therapies [8]. However, their weak immunogenicity and inadequate lymph node targeting pose challenges to their direct use as tumor vaccines [9]. In response to these challenges, scientists have employed various chemical [10] and biological engineering [11] techniques to enhance the antitumor immune response elicited by tEVs. However, the intricate design and laborious preparation processes have introduced new issues, such as systemic immunotoxicity, elevated production expenses, and product instability [12]. Therefore, there is an urgent need to prepare simple and efficient vaccines for precise tumor treatment.

It is well established that viral components, recognized by the immune system as “exogenous danger signals,” can act as powerful vaccine adjuvants to augment antitumor immunity. Furthermore, an effective immune response to virus-infected cells involves the concurrent activation of both innate and adaptive immune responses against both viruses and tumors [13], suggesting the potential advantage of a multiantigenic vaccine in cancer immunotherapy [14]. Vesicular stomatitis virus (VSV) as a natural oncolytic virus that can selectively replicate in type I interferon (IFN) response-defective or reduced tumor cells [15]. During the replication of VSV in tumor cells, a large amount of envelope glycoprotein VSVG is transferred to the cell membrane surface following modification and maturation in the Golgi apparatus [16]. Meanwhile, VSVG acting as an agonist for Toll-Like Receptor 4 (TLR4), enhances the specific recognition and elimination of tumor cells by immune cells [17]. Additionally, recent evidence indicates that VSV infection can induce immunogenic cell death (ICD), leading to the exposure of calreticulin on the cell surface and the release of danger-associated molecular patterns (DAMPs) [18].

In this study, leveraging the infectious nature of VSV against tumor cells, we developed a “self-adjuvant” multiantigenic nanovaccines designed to elicit both antiviral and antitumor immune responses for cancer therapy. As illustrated in Scheme 1, infecting 4T1 tumor cells with VSV leads to viral replication and induces ICD, causing the concurrent display of VSVG and CRT on the tumor cell surface. Following the collection and subcutaneous administration of extracellular vesicles (vEVs) derived from virus-infected tumor cells, their inherent tumor-targeting property, derived from the parent tumor cells, ensures effective accumulation within tumors. Here, the low pH-sensitive VSVG transitions to an unfolded fusion state, facilitating membrane fusion between vEVs and tumor cells, thereby enhancing macrophage recognition and phagocytosis of tumor cells. Additionally, the vEV surface-exposed CRT activates the “eat-me” signaling pathway, improving their detection and uptake by

dendritic cells (DCs). Consequently, DC maturation is induced, leading to the activation of both antiviral and antitumor T cells for a synergistic antitumor effect. This innovative system triggers robust anti-tumor immunity in mouse models of triple-negative breast cancer, significantly inhibiting tumor growth and extending survival time, particularly when combined with the immune checkpoint inhibitor aPD-1. Therefore, this research provides a straightforward and convenient approach for the creation of a novel tumor vaccine, offering a highly effective and safe treatment option for solid tumors.

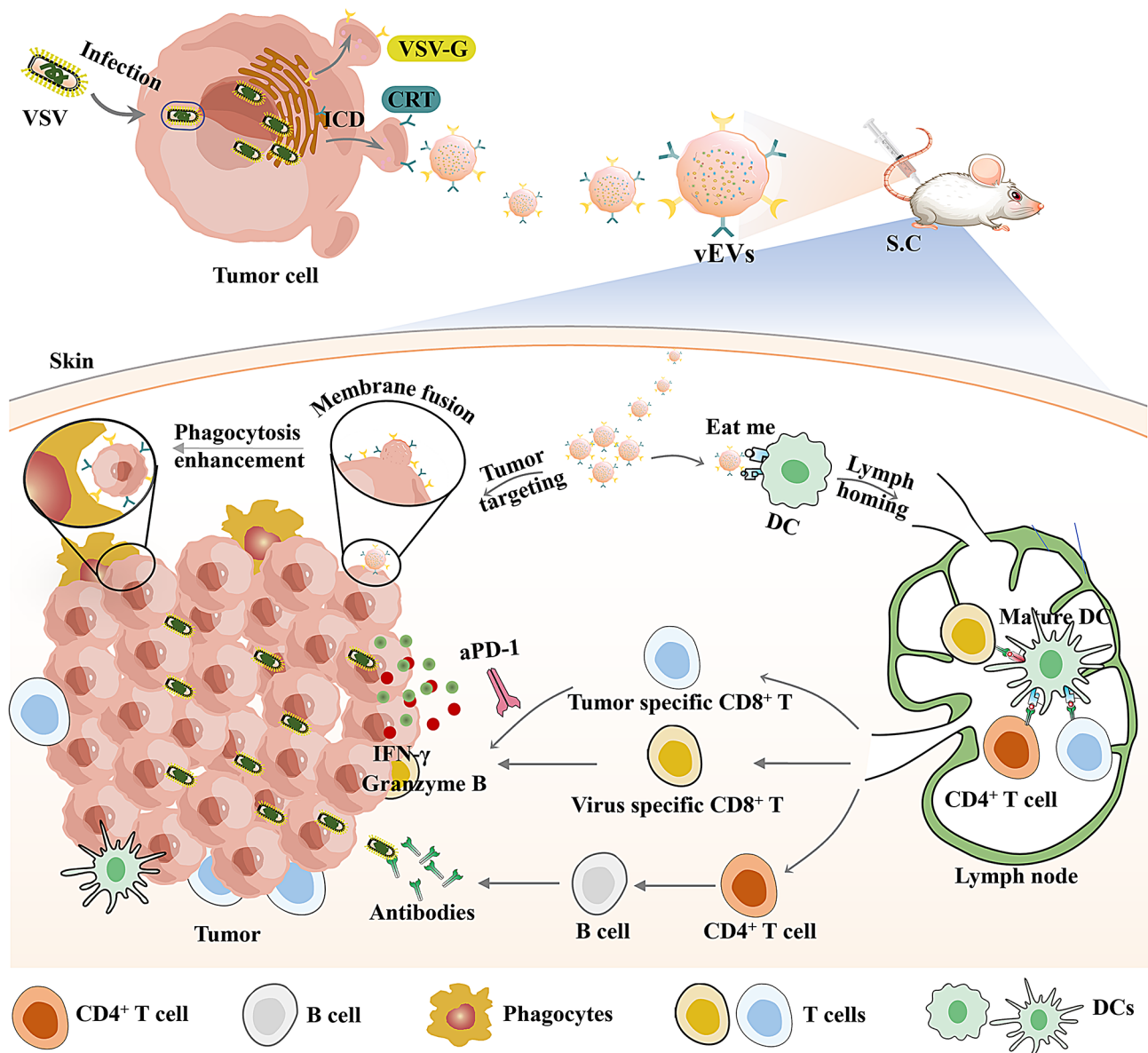
## Methods

### Cell culture

Cell lines including African green monkey kidney (Vero), human hepatocellular carcinoma (HepG2), murine melanoma (B16), colorectal carcinoma (CT26), and mammary carcinoma (4T1) were sourced from the Peking Union Medical College Hospital. These cell types were maintained in Dulbecco's Modified Eagle Medium (DMEM) from Gibco, enriched with 10% fetal bovine serum (FBS) supplied by Gibco, along with 100 IU/mL of penicillin and 100 µg/mL of streptomycin, both also from Gibco. The cells were incubated at 37 °C under a humidified environment with a 5% CO<sub>2</sub> atmosphere.

Bone marrow-derived macrophages (BMDMs) were generated from female C57BL/6 mice, aged 4–6 weeks. First, bone marrow was extracted by flushing the tibias and fibulas of the mice with phosphate-buffered saline (PBS), and then red blood cells were lysed using ammonium-chloride-potassium lysing buffer (ACK lysis buffer). Subsequently, the remaining cells were pelleted by centrifugation at 300 × g for 5 min. These cells were cultured in RPMI 1640 medium supplemented with 10% FBS, 100 µg/mL penicillin, 100 µg/mL streptomycin, 25 ng/mL murine macrophage colony-stimulating factor (M-CSF) for 6 days.

Bone marrow-derived dendritic cells (BMDCs) were produced using females of the C57BL/6 strain, aged 4–6 weeks, according to the following protocol. Initially, bone marrow was harvested by flushing the tibias and fibulas of the mice with PBS, followed by the lysis of red blood cells using ammonium-chloride-potassium lysing buffer (ACK lysis buffer). Afterward, the residual cells were pelleted by centrifugation at 300 × g for a duration of 5 min. These cells were then seeded at a density of  $5 \times 10^5$  cells per well in 24-well plates and cultured in RPMI 1640 medium supplemented with 10% FBS, 100 µg/mL penicillin, 100 µg/mL streptomycin, 20 ng/mL of murine interleukin-4 (IL-4) supplied by Peprotech, and 20 ng/mL of murine granulocyte-macrophage colony-stimulating factor (GM-CSF) also from Peprotech, for a period of 7 days.



**Scheme 1** Schematic illustration of the preparation and antitumor effect of vEVs

T lymphocytes were derived from the spleens of 4-6-week-old female C57BL/6 mice. The spleens were excised and mechanically disrupted to create a single-cell suspension. This suspension was then passed through 75 μm filters to remove any clumps. Following two washing steps, the red blood cells were eliminated by incubation with ACK lysis buffer. The remaining cells were sedimented by centrifugation at  $800 \times g$  for a period of 5 min. The purified cells were subsequently cultured at a density of  $5 \times 10^5$  cells per well in 24-well plates, using RPMI 1640 medium as the culture medium.

#### Assessment of VSV replication and viral infectious capacity

VSV was amplified in monolayer cultures of Vero cells maintained at 37 °C in 1640 medium supplemented with 2% FBS. The virus propagation was conducted for a period of 24 h. Subsequent to three cycles of freeze-thaw to release the virus particles, cellular debris was eliminated by centrifugation at 5,000 rpm for 20 min at 4 °C. The supernatant, rich in VSV, was then harvested and preserved at -80 °C for future use.

Vero cells were seeded into 96-well plates at a density of  $5 \times 10^5$  cells per well. Following the achievement of 60% confluence, the VSV was serially diluted tenfold, ranging from  $10^{-1}$  to  $10^{-10}$ , in 1640 medium supplemented with 2% FBS. These diluted virus preparations were then introduced to the cell cultures for an infection period of

roughly 2 days. The 50% tissue culture infectious dose (TCID<sub>50</sub>) was determined by quantifying the number of wells exhibiting cytopathic effect (CPE) on the Vero cells, utilizing the Reed and Muench method as described previously [19].

#### Isolation and preparation of tEVs and vEVs

Cells of the 4T1 line, both those infected with VSV at a multiplicity of infection (MOI) of 0.1 and the corresponding uninfected controls, were incubated at 37 °C for a duration of 48 h. Following the infection period, cellular material and debris were separated by centrifugation at 1000 × g for 10 min and then at 14,000 × g for 1 min at 4 °C. The resulting supernatants containing tEVs and vEVs were further purified by centrifugation at 14,000 × g for 1 h at 4 °C. The pelleted vesicles were then subjected to a washing step and resuspended in PBS. tEVs and vEVs were subsequently filtered through a 0.1 μm polymeric membrane (Nucleopore Track-Etch Membrane, Whatman, UK) using an extruder (Avanti Polar Lipids, USA) and finally stored at -80 °C. The concentrations of tEVs and vEVs were quantified using a bicinchoninic acid (BCA) protein assay kit (Solarbio PC0020).

#### Characterization of tEVs and vEVs

To investigate the morphology of tEVs and vEVs, 10 μL of each sample were placed onto carbon-coated copper grids. Excess liquid was removed by blotting with filter paper. The samples on the grids were then subjected to negative staining using 1% (v/v) uranyl acetate. After staining, the grids were examined under transmission electron microscopy (TEM), specifically using a JEOL JEM-1400 microscope.

The mean particle size and ζ potential measurements for tEVs and vEVs were obtained using a Zetasizer Nano ZS dynamic light scattering (DLS) apparatus (Malvern Instruments, UK). To assess the stability of both tEVs and vEVs, these extracellular vesicles were incubated in either PBS or 10% fetal bovine serum (FBS) for a period of 7 days at 4 °C. Following this incubation, DLS was employed to monitor changes in particle size and to determine the particle dispersion index (PDI) distribution.

#### Colocalization imaging of VSVG and exosomes in vEVs

Exosome membranes and VSVG preparations for vEVs were individually labeled with 1,1'-dioctadecyl-3,3,3',3'-tetramethylindocarbocyanine perchlorate (DiI, Thermo Fisher Scientific) and FITC-conjugated anti-VSVG antibody (VSVG, Thermo Fisher Scientific) for a duration of 30 min at room temperature. Unbound fluorescent molecules were separated using ultrafiltration (10 kDa, 5000 × g for 5 min). Subsequently, the DiI and FITC-labeled vEVs were introduced into a confocal dish (MatTek) and visualized using a laser scanning confocal microscope

(CLSM, Nikon, Japan). For imaging, the FITC-conjugated anti-VSVG antibody was excited at a wavelength of 488 nm, while DiI was excited at 549 nm.

#### SDS-PAGE and western blotting analysis

tEVs and vEVs were combined with loading buffer and subjected to heat denaturation at 100 °C for 10 min to disrupt protein structures. Thereafter, 10 μL of the mixture, containing 20 μg of protein, was loaded into the wells of a 10% SDS-PAGE gel. Following electrophoresis, the separated proteins were transferred onto a nitrocellulose (NC) membrane. The NC membrane was then blocked with 5% bovine serum albumin (BSA) for 2 h and incubated overnight at 4 °C with primary antibodies, including anti-CD63 (Abcam, ab217345), anti-ALIX (Abcam, ab275377), anti-VSVG (Abcam, ab138512), anti-CRT (Abcam, ab212059), and anti-β-actin (Bioss, bs-0061R). The next day, the membrane was washed three times with PBST (phosphate-buffered saline with 0.1% Tween 20) and incubated with a horseradish peroxidase (HRP)-conjugated goat anti-rabbit IgG secondary antibody (Bioss, bs-0295G-HRP) for 2 h. After additional washes with PBST, the membrane was developed using an enhanced chemiluminescence (ECL) reagent (Thermo Scientific, 35055) and visualized with a chemiluminescence detection system (Bio-Rad, USA).

#### In vitro cellular uptake of vEVs by homologous tumor cells and BMDCs

The BMDCs or tumor cells were seeded at a density of  $2 \times 10^5$  cells/mL in confocal dishes and incubated for 24 h. DiO-labeled tEVs or vEVs were then added to the BMDCs/tumor cells and incubated for an additional 2 h. Subsequently, tumor cells were stained with WGA-Cy5 for 15 min at room temperature, while BMDCs were stained with PE-conjugated anti-CD11c antibody, for a period of 30–45 min at 4 °C. After three washes with PBS, the cells were fixed with 4% paraformaldehyde at room temperature and washed again with PBS. To label the cell nuclei, Hoechst 33,342 (Beyotime, C1022) was added for 15 min at room temperature and imaging with a confocal laser scanning microscope (CLSM).

For the quantitative analysis of the internalization efficiency of vEVs by BMDCs or homologous tumor cells, cells were seeded at a density of  $5 \times 10^5$  cells/mL in 24-well plates and incubated for 24 h. After that, they were co-incubated with DiO-labeled tEVs or vEVs at a concentration of 50 μg/mL for 2 h, then the cells were collected and the fluorescence intensity was measured using a flow cytometer (BD FACSAria™ III, USA) with excitation at 488 nm. The data obtained were analyzed using FlowJo software (Tree Star, USA).

### Phagocytosis assay

4T1-GFP cells were co-incubated with tEVs or vEVs at 37 °C for 2 h under varying pH conditions. After three washes with PBS, these cells were added into CD11b-labeled BMDMs at 37 °C for 2 h. After three washes with PBS, the cells were added into a confocal dish (MatTek) and visualized using a laser scanning confocal microscope (CLSM, Nikon, Japan). For imaging, the 4T1-GFP cells were excited at a wavelength of 488 nm, while CD11b-labeled BMDMs were excited at 561 nm.

For the quantitative analysis of the phagocytosis efficiency of 4T1-GFP cells by BMDMs, 4T1-GFP cells were seeded at a density of  $5 \times 10^5$  cells/mL in 24-well plates and incubated for 24 h. After that, they were co-incubated with tEVs or vEVs at a concentration of 50 µg/mL for 2 h under varying pH conditions, then the cells were collected and added into CD11b-labeled BMDMs at 37 °C for 2 h. The fluorescence intensity GFP<sup>+</sup>CD11b<sup>+</sup> BMDMs was measured using a flow cytometer (BD FACSAria™ III, USA). The data obtained were analyzed using FlowJo software (Tree Star, USA).

### CCK-8 cytotoxicity assay

The 4T1 cells or DCs were plated at a density of 5000 cells per well in 96-well plates and incubated for 24 h. Following this incubation period, the cells were exposed to PBS, tEVs, or vEVs for an additional 48 h. The optical density (OD) of each well was then measured at a wavelength of 450 nm using an automated microplate reader (BioTek Instruments, Inc.). To determine cell viability, the absorbance ratios of the cells treated with various formulations were compared to the absorbance of cells incubated with culture medium alone, which served as the control.

### In vivo evaluation of tumor homologous targeting

DiR-labeled tEVs or vEVs were prepared for administration. BALB/c mice were divided into two groups and each mouse received a subcutaneous injection of 100 µg of labeled EVs at the base of the tail. Fluorescence imaging was performed at intervals ranging from 0 to 96 h post-injection using an IVIS imaging system (PerkinElmer, USA).

### In vitro assessment of maturation in BMDCs and activation of T lymphocytes

To evaluate the maturation status of BMDCs, cells were cultured at a concentration of  $5 \times 10^5$ /mL and treated with PBS, tEVs, or vEVs for a period of 48 h. Following treatment, the cells were incubated with PE-conjugated anti-CD86 antibody (Biolegend, 105105) and FITC-conjugated anti-CD80 antibody (Biolegend, 104706) for 30–45 min at 4 °C. After staining, the cells were washed with cold PBS to remove unbound antibodies, and the fluorescence signal was then quantified using a flow

cytometer. In parallel, the culture supernatants were harvested, and the levels of cytokines IL-6 (Biolegend, 430517) and TNF-α (Biolegend, 430204) were measured using ELISA kits. All experimental conditions were conducted in triplicate for analysis.

To gauge the activation status of splenic T lymphocytes, BMDCs were pre-treated as previously described. Following a 48 h pre-treatment, these BMDCs were then co-cultured with T lymphocytes for an additional 24 h. Subsequently, the cells were washed three times with PBS to remove any non-adherent material and then incubated with APC-conjugated anti-CD3 (Biolegend, 155606), FITC-conjugated anti-CD8 (Biolegend, 100804), and PE-conjugated anti-CD69 antibodies (Biolegend, 104508) for 30–45 min at 4 °C. After staining, the cells were washed with cold PBS to remove unbound antibodies and analyzed by flow cytometry to assess CD69 expression. Concurrently, the culture supernatants were collected, and the concentrations of cytokines IFN-γ (Biolegend, 430807) and Granzyme B (Biolegend, 439207) were quantified using ELISA kits. All experimental groups were analyzed in triplicate to ensure data reliability.

### Tumor inhibition assays

All animal studies were conducted in accordance with the guidelines and ethical standards approved by the Experimental Animal Committee of the Beijing Institute of Technology. Female BALB/c mice, aged 6 weeks, were obtained from Vital River Laboratory Animal Technology Co, Ltd.

Mice were initially inoculated with  $1 \times 10^6$  4T1 cells subcutaneously into the right flank. Treatment began once the tumors reached a volume of approximately 100 mm<sup>3</sup>. The mice were then randomly assigned to five groups ( $n=6$  per group) and received subcutaneous injections at the tail base with PBS, tEVs, vEVs, aPD-1, or vEVs combined with aPD-1 on day 7. An additional intravenous dose via the tail vein was administered on day 12. The tumor dimensions and body weight of the mice were recorded every other day. Tumor volume was calculated using the formula:  $(\text{length} \times \text{width}^2) / 2$ . Mice were euthanized when the tumor volume exceeded 1000 mm<sup>3</sup>.

For the analysis of immune cells, the draining lymph nodes (DLNs) and tumor tissues were surgically removed from the mice as previously outlined. The excised tissues were then homogenized in cold PBS to create single-cell suspensions. The resulting cell suspensions were aliquoted for the analysis of various immune cell subsets. To assess DCs maturation, lymph node cells were labeled with antibodies specific to CD80 and CD86 markers. For cytotoxic T lymphocyte (CTL) analysis, tumor-derived cells were stained with antibodies against CD3, CD8, and IFN-γ. Following staining, the cells were washed three

times with PBS to remove unbound antibodies before being analyzed by flow cytometry.

To assess tumor growth inhibition, mice were euthanized, and tumor tissues were excised for immunohistochemical analysis. The tumor specimens were fixed in 4% paraformaldehyde and subsequently sectioned. These sections were then subjected to staining for the nucleus-related antigen Ki67, which is a marker of cell proliferation, as well as terminal deoxynucleotidyl transferase-mediated deoxyuridine triphosphate nick end labeling (TUNEL) staining, which detects apoptotic cells.

### Plaque reduction neutralisation test (PRNT)

The serum samples were collected from immunized mice that had been immunized via treatment with tEVs or vEVs (100 µg/mouse) for a period of 14 days. To quantify the neutralizing antibodies against VSV, a plaque reduction neutralization test (PRNT) was conducted. Initially, Vero cell monolayers were seeded in 12- or 24-well plates (Corning) and cultured at 37 °C in a CO<sub>2</sub> incubator 24 h before viral infection. The serum samples were serially diluted, combined with VSV, and subjected to plaque assays as previously outlined [20]. Neutralizing antibody titers (PRNT<sub>50</sub>) were determined as the highest serum dilution achieving a 50% reduction in viral plaque counts compared to the control.

### Statistical analysis

The data are depicted as mean values plus or minus the standard error, unless specified otherwise, and were processed using GraphPad Prism 8 software. Statistical significance was determined by performing an unpaired, two-tailed Student's t-test for comparisons between two

groups, and a one-way analysis of variance (ANOVA) with Tukey's post-hoc test for multiple comparisons. A significance level of \* $P < 0.05$ , \*\* $P < 0.01$ , \*\*\* $P < 0.001$ , or \*\*\*\* $P < 0.0001$  was used to denote statistical significance, with n.s. indicating non-significant differences.

## Results and discussion

### Preparation and characterization of vEVs

To generate vEVs, 4T1 cells were initially infected with VSV, and the vEVs were isolated from the culture supernatant using ultracentrifugation. Transmission electron microscopy (TEM) revealed the classical exosome cup-like morphology for vEVs (Fig. 1a). The similar size and zeta potential were observed in both tEVs and vEVs (Fig. 1b-c). Western blot analysis showed that vEVs expressed exosome markers CD63 and ALG-2-interacting protein X (ALIX), confirmed the successful isolation of exosomes (Fig. 1d). Moreover, the expression of CRT and VSVG increased in the vEVs compared to the tEVs (Fig. 1d) due to the infection of VSV to parent 4T1 cells. Notably, the presence of VSVG in western blot, which exhibited robust colocalization with DiI-labeled vEVs in confocal laser scanning microscopy (CLSM), suggests that vEVs might acquire certain biological characteristics of VSV (Fig. 1g). Finally, vEVs demonstrated the desired stability, with no detectable changes in particle size observed following a 7-day storage period in 10% FBS (v/v) (Fig. 1e-f).

### In vitro targeting performance of vEVs

After successfully preparation, we then attempted to estimate the vEVs uptake by the parent cells. We comparatively investigated the uptake of vEVs (labeled with DiO)

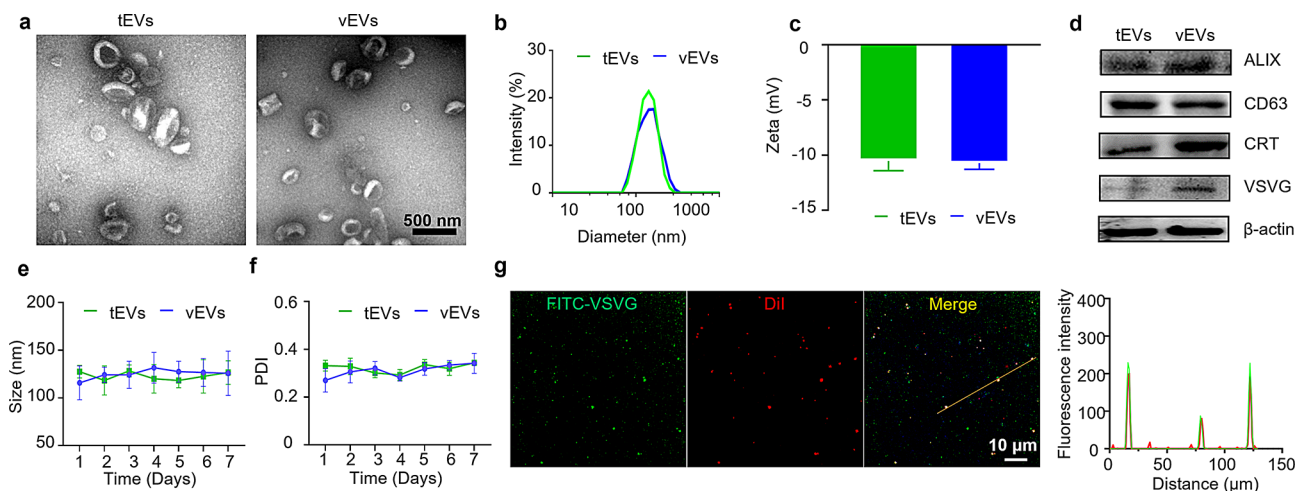


**Fig. 1** Preparation and characterization of vEVs. **(a)**, TEM imaging of the tEVs and vEVs. **(b)**, **(c)**, Average particle size **(b)** and  $\zeta$  potential **(c)** distribution of tEVs, vEVs, as analyzed by DLS. **(d)**, Western blot analysis of CRT and VSVG expression in different EV formations. **(e)**, **(f)**, Size **(e)** and PDI **(f)** distribution of vEVs stored in 10% FBS (v/v) for 7 days. **(g)**, Fluorescence colocalization imaging of vEVs. VSVG is depicted in green, exosomes are depicted in red, and the fluorescence intensity of both VSVG and membrane of vEVs is indicated by orange lines. Data are presented as mean  $\pm$  S.D. ( $n = 3$  biologically independent samples)

by different cells, including mouse colon cancer (CT26), human hepatocellular carcinoma (HepG2), mouse melanoma (B16), and 4T1 cells (the source of vEVs). The uptake behaviors were analyzed using CLSM and flow cytometry. As shown in Fig. 2a and b, vEVs showed negligible uptake by CT26, HepG2, and B16 cells. In contrast, vEVs induced a much higher uptake efficiency in 4T1 cells, with 3.8–11.4 times of the mean fluorescence intensity (MFI) higher than that of others cells, revealing the parent cells-specific homing preference of vEVs.

The VSVG has been reported to be sensed by the innate immune cells as a pathogen-associated molecular patterns (PAMP) [21]. Considering the low pH-sensitive membrane fusion activity of VSVG [22] and the acidic environment of tumors, we exposed 4T1-GFP cells to vEVs under varying pH conditions for 2 h and then investigated whether vEV-mediated xenogenization could enhance the *in vitro* phagocytic activity of BMDMs towards tumor cells. Our result showed that 4T1-GFP cells treated with vEVs at pH 6.8 were more efficiently engulfed by BMDMs than the respective controls, suggesting that this viral PAMP on the tumor cell surface can augment the phagocytic capabilities of immune cells to tumor cells (Fig. 2c and Fig. S1).

In addition to the improved uptake of vEVs by their parent cells, we next assessed the uptake capacity of vEVs by DCs. Given that the cell surface-exposed CRT provides an “eat me” signal has been reported responsible for specific recognition and phagocytic uptake of nanoparticles by antigen-presenting cells (APCs), primarily DCs, the increased CRT on vEVs should promote the uptake of vEVs by DCs. To assess this point, BMDCs were treated with DiO-labeled vEVs or tEVs. As expected, a large number of vEVs with marked fluorescence were observed in BMDCs (Fig. 3a). The flow cytometry data further indicated that BMDCs demonstrated a 1.4-fold increase in the uptake of vEVs as compared to tEVs (Fig. 3b), confirming the presence of CRT on the vEVs significantly enhance the internalization efficiency of vEVs by BMDCs. Additionally, both of vEVs and tEVs showed favorable biocompatibility, with negligible cytotoxicity towards homotypic 4T1 cells and BMDCs (Fig. 3c-d).

To further evaluate the targeting capacity of vEVs *in vivo*, we subcutaneously injected DiR-labeled vEVs or tEVs into 4T1-tumor BALB/c mice and the determined the targeting accumulation via time-elapsd fluorescence imaging using IVIS imaging system. As shown in Fig. 3e, both vEVs and tEVs exhibited similar kinetic profiles,

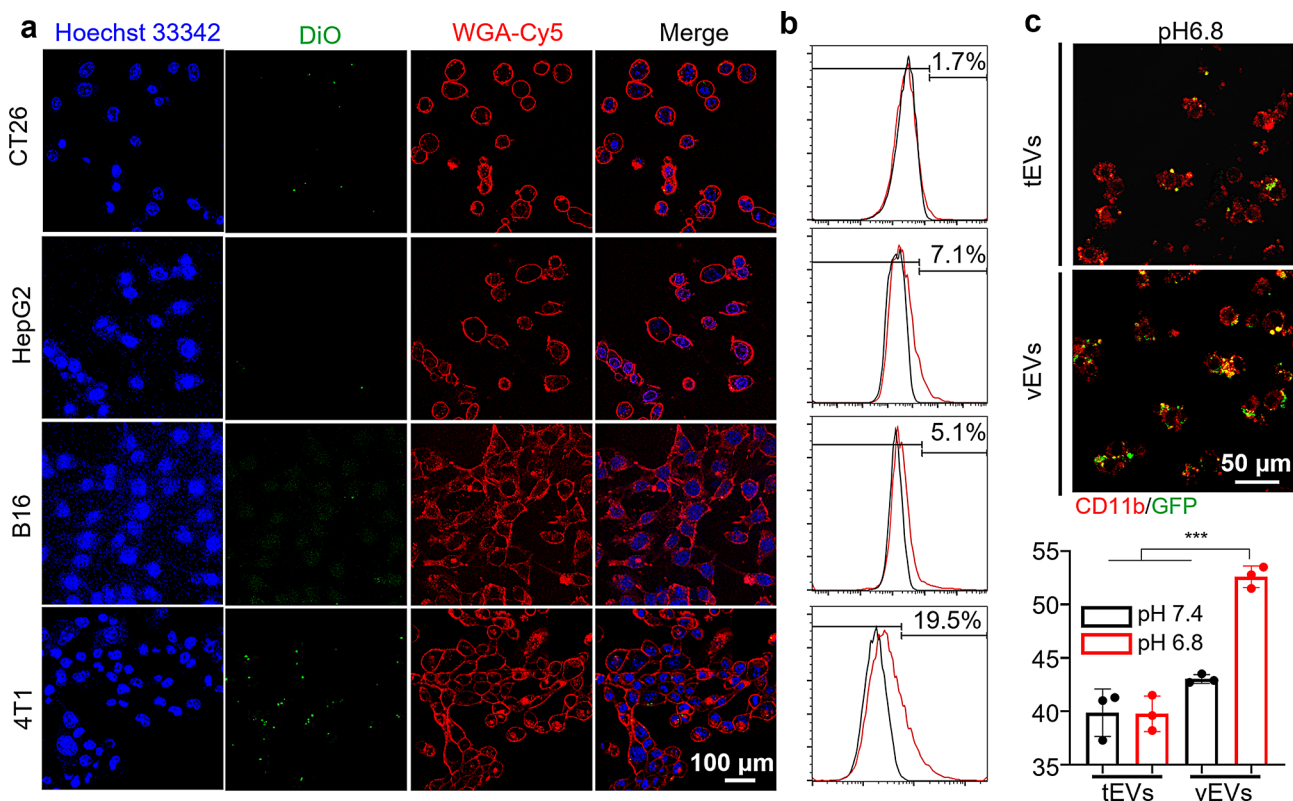


**Fig. 2** Homologous targeting of vEVs and enhanced phagocytic capabilities of macrophages. (a), (b), Fluorescence imaging (a) and flow cytometric analysis (b) of the cellular uptake of vEVs by 4T1, CT26, B16, or HepG2 cells (green: DiO-labeled vEVs, blue: Hoechst 33342-labeled nucleus, red: WGA-Cy5-labeled cell membrane). (c), Fluorescence imaging and flow cytometric analysis of phagocytic activity of BMDMs towards tumor cells. Data are presented as mean  $\pm$  S.D. ( $n=3$  biologically independent samples)

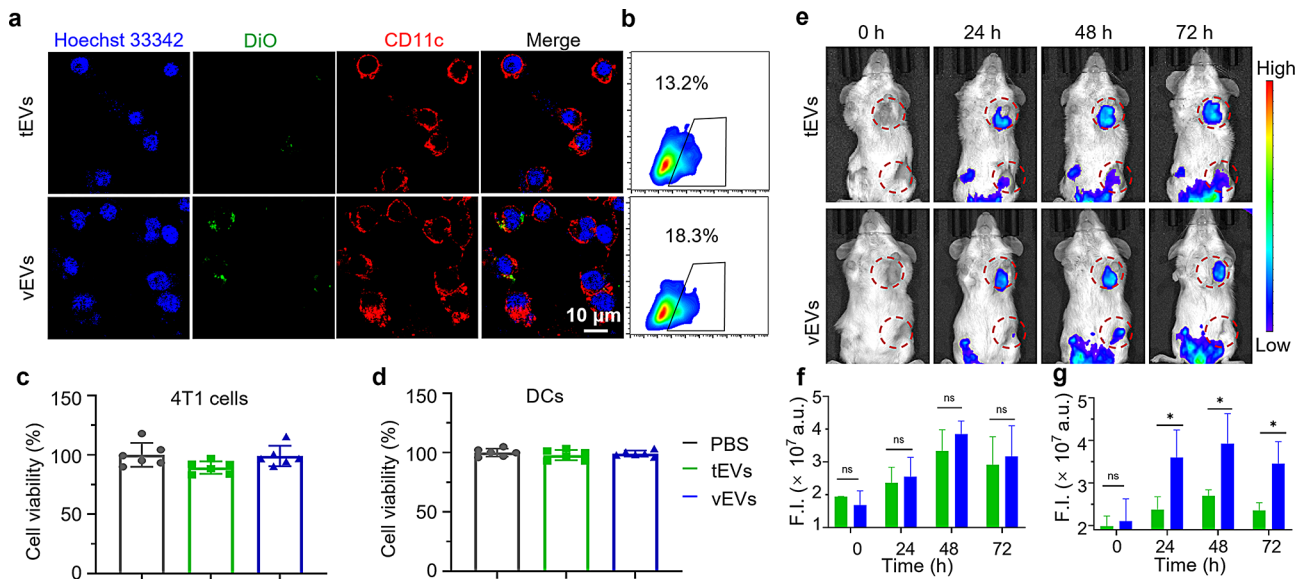


**Fig. 3** Validation of the homologous tumor-cell and DC dual-targeting properties of vEVs. **(a), (b)**, Fluorescence imaging **(a)** and flow cytometric analysis **(b)** of the cellular uptake of tEVs or vEVs by BMDCs (green: DiO-labeled vEVs, blue: Hoechst 33342-labeled nucleus, red: PE-conjugated anti-CD11c-labeled BMDCs). **(c), (d)**, Relative cell viability of 4T1 cells **(c)** and BMDCs **(d)** after incubation with different formulations for 48 h. **(e)**, Representative in vivo fluorescence imaging of 4T1 tumor-bearing mice at the indicated time points after subcutaneous injection with DiR-labeled tEVs or vEVs. **(f), (g)**, Fluorescence intensity (F.I.) of 4T1 tumors **(f)** and LNs **(g)** at the indicated time points, Data are presented as mean  $\pm$  S.D. ( $n=3$  biologically independent samples)

with fluorescence signals at the tumor and lymph node (LN) sites peaking at 48 h post-injection. Notably, the fluorescence signals of vEVs in tumor sites were comparable to that of tEVs (Fig. 3f and Fig. S2). While vEVs demonstrated a 2.0-fold increase in accumulation within the lymph nodes (LNs) compared to tEVs (Fig. 3g and Fig. S2). This enhanced accumulation in LNs is likely due to the concurrent presence of VSVG and CRT on the vEV surface. The data suggest that vEVs not only preserve the tumor-targeting efficacy of tEVs but also significantly augment their capacity to target lymph nodes.

#### In vitro DC maturation and cytotoxic T cells activation

Taking into account the enrichment of virus-related elements, such as viral proteins and gene segments, within extracellular vesicles derived from tumor cells during VSV infection [23], it is theoretically plausible that vEVs treatment could facilitate the maturation of DCs. For confirmation, BMDCs were treated with vEVs or tEVs for 48 h, after which the expression levels of the mature DC markers CD80 and CD86 were measured. As shown in Fig. 4a-b and Figure S3, compared to the PBS group, the expression of costimulatory molecules CD80 and CD86 in BMDCs were upregulated in the tEVs group. Notably, the expression of these molecules further increased following vEVs treatment, demonstrating a 2.5-fold and 3.9-fold enhancement compared to the tEVs groups, respectively, indicating the superior ability of vEVs to promote DC maturation. The activation of cytotoxic T cells was also assessed by detected the expression of

activation markers CD69. Consistent with the data on DC maturation, the vEVs group exhibited the highest percentage of CD69<sup>+</sup> T cells (Fig. 4c and Fig. S4). Correspondingly, levels of tumor necrosis factor- $\alpha$  (TNF- $\alpha$ ), interleukin-6 (IL-6), Interferon- $\gamma$  (IFN- $\gamma$ ), and Granzyme B in the vEVs group were significantly higher than those in the PBS and tEVs groups, underscoring the enhanced efficacy of DC maturation and T cell activation following vEVs administration (Fig. 4d-g).

#### Tumor inhibitory effects of vEVs

These promising findings described above motivated us to further evaluate the immune-activation effects of vEVs in vivo. After administering various vaccine formulations, we examined the immune cell profiles within tumors via flow cytometry, revealing a substantial enhancement in the proportions of mature DCs (CD11c<sup>+</sup>CD80<sup>+</sup>CD86<sup>+</sup>) and CTLs (CD3<sup>+</sup>CD8<sup>+</sup>IFN $\gamma$ <sup>+</sup>) (Fig. 5a-b and Fig. S5-S6). Specifically, the injection of vEVs resulted in intratumoral CD80<sup>+</sup>CD86<sup>+</sup> DCs and CD8<sup>+</sup>IFN $\gamma$ <sup>+</sup> T cells increasing by 1.75- and 1.4-times, respectively, indicating that vEV therapy markedly elevated anti-tumor immune response. Moreover, high titers of total IgG antibodies and neutralizing antibodies were detected in mouse serum (Fig. 5c-d and Fig. S7), indicating that antiviral immunity was also highly activated. Furthermore, we investigate the mechanisms behind the immune activation induced by vEVs using RNA sequencing techniques. Our findings revealed that vEV treatment in tumors led to a significant upregulation of various genes associated with

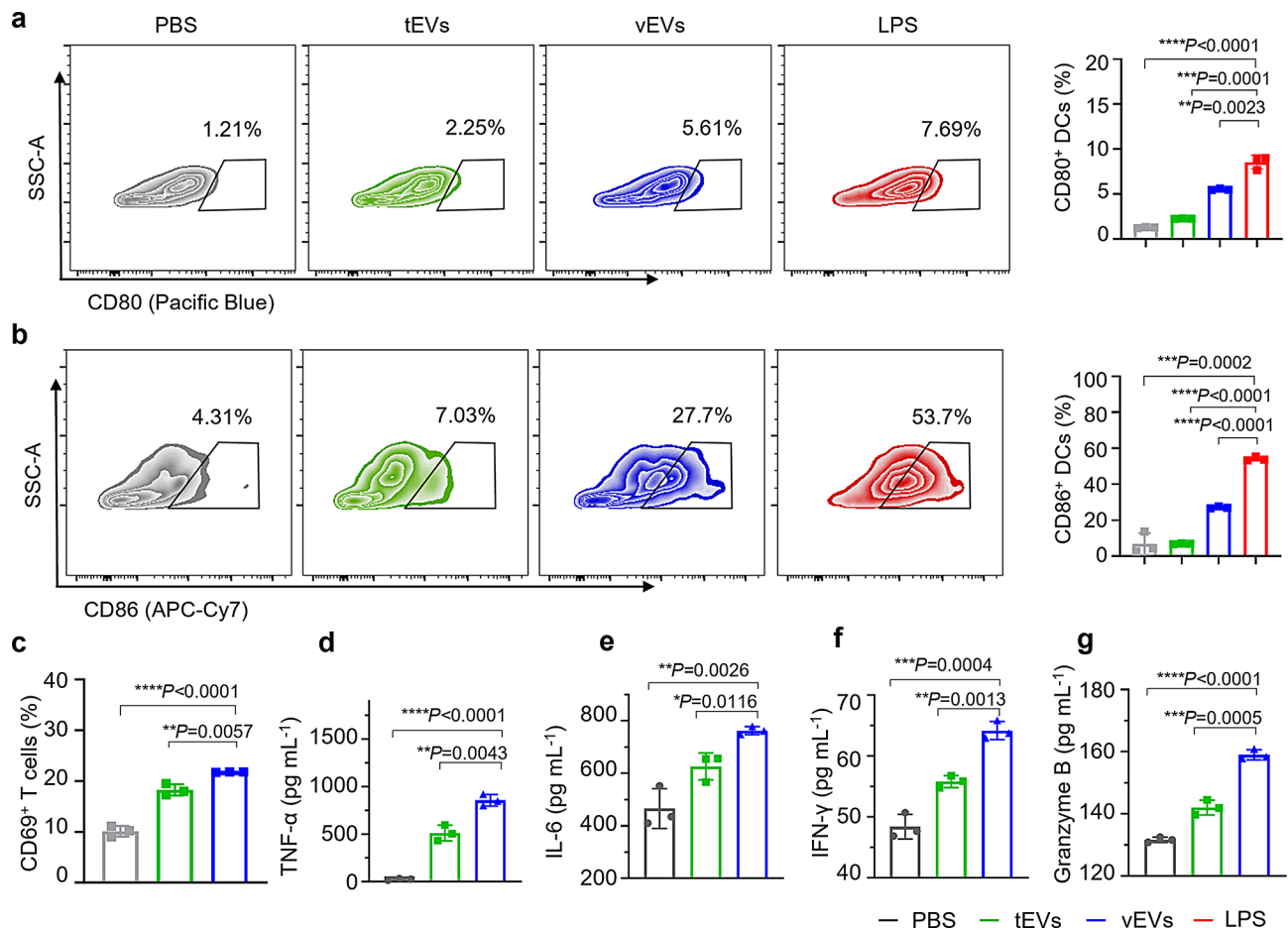


**Fig. 4** vEVs induced the DC maturation and T-cell activation. **(a), (b)**, Flow cytometric analysis of CD80 and CD86 expression in BMDCs after treatment with different formulations for 48 h. **(c)**, Flow cytometric analysis of expression levels of CD69<sup>+</sup> T cells after treatment with different formulation-activated BMDCs for another 24 h. **(d), (e)**, Release of the TNF- $\alpha$  **(d)** and IL-6 **(e)** by BMDCs after coculture with different formulations for 48 h. **(f), (g)**, Release of IFN- $\gamma$  **(f)** and granzyme B **(g)** cytokine by T cells after treatment with different formulation-activated BMDCs. Data are presented as mean  $\pm$  S.D. ( $n=3$  biologically independent samples)

immune activation, including CXCL10, CD40, and TLR9, concurrently with a reduction in the expression of genes that promote immunosuppression, such as MMP10 and VEGFA. Additionally, the expression of cancer-promoting genes like TGFB2 and ARG1 was decreased. The Kyoto Encyclopedia of Genes and Genomes (KEGG) pathway enrichment analysis highlighted a substantial activation of pathways involving viral protein interaction with cytokine-cytokine receptor interaction, Toll-like receptor signaling, and chemokine signaling in the vEV-treated tumors compared to the PBS-treated group (Fig. S8). Generally, these results provide a solid foundation for triggering synergistic antitumor and antiviral immune responses for the treatment of cancers in vivo.

Therefore, we proceed to assess the therapeutic efficacy of the vaccine formulations in vivo. For this purpose, 4T1 tumor-bearing C57BL/6 mice were randomly allocated into four groups and administered with different vaccine formulations (Fig. 5e). The vEVs group exhibited a

more significant inhibition of tumor growth than both the PBS and tEVs groups. Notably, the combination therapy of vEVs with anti-PD-1 yielded a substantial tumor-suppressive effect, resulting in a 72.5% inhibition of tumor growth and improved overall survival rates (Fig. 5f-g and Fig. S9). In contrast to the mice in the other groups, which died within 35 days, more than 80% of the mice in the vEVs plus anti-PD-1 group survived beyond this period (Fig. 5h-i). TUNEL staining and Ki67 analysis further indicated a considerable increase in apoptotic cells within the tumor tissues of the vEVs+anti-PD-1 group (Fig. 5j-k). H&E staining of vital organs including the heart, liver, spleen, lungs, and kidneys, revealed no significant damage (Fig. S10). Moreover, no significant differences were observed in body weight and serum biochemistry parameters, confirming the favorable safety profile of vEVs for antitumor treatment (Fig. S11-S12).

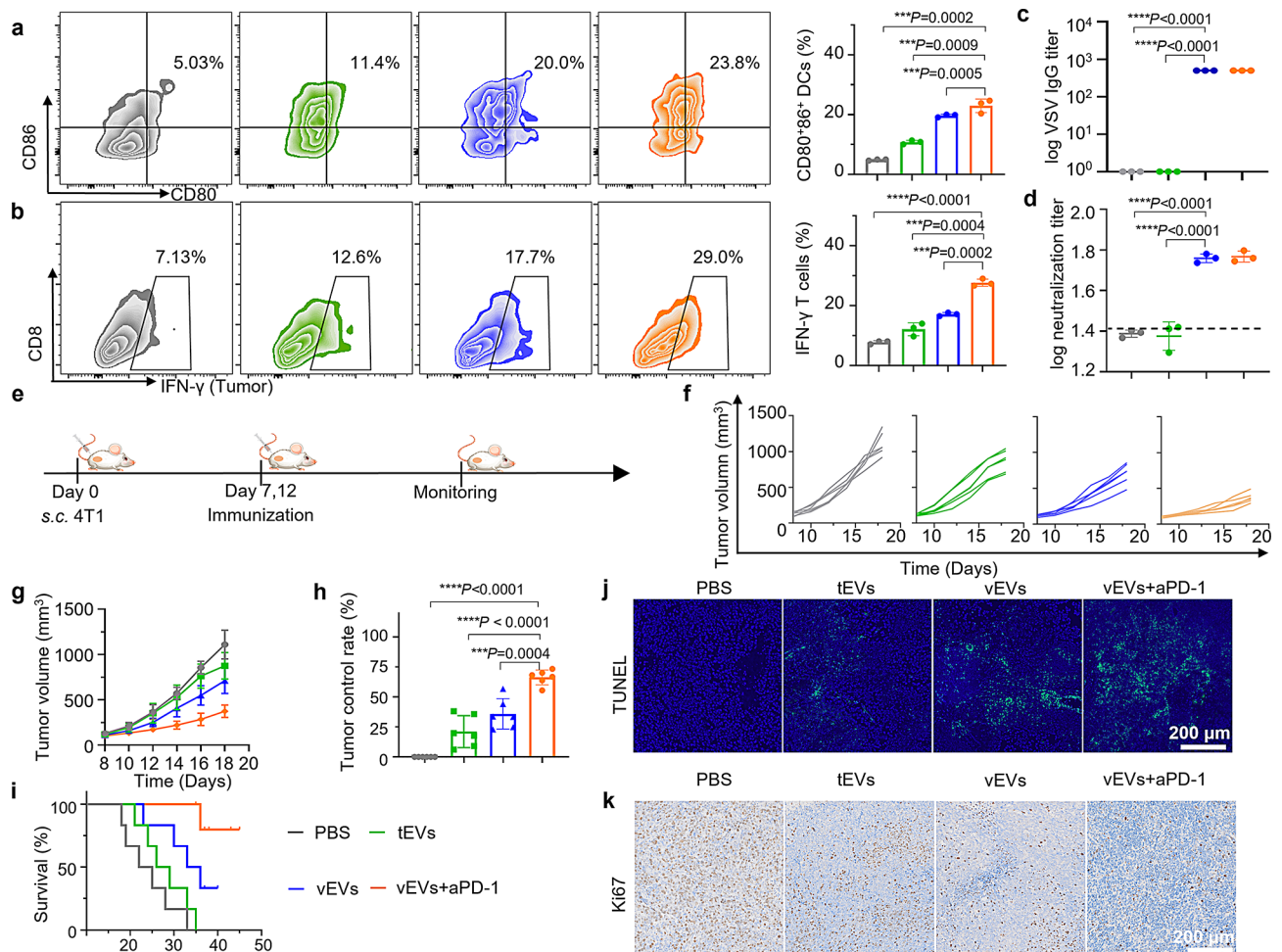


**Fig. 5** Combined treatment with vEVs and anti-PD-1 effectively induces antitumor immunity. **(a)**, Flow cytometric analysis of the percentages of CD80<sup>+</sup>CD86<sup>+</sup> DCs in DLNs. **(b)**, Flow cytometric analysis of the percentages of IFN- $\gamma$ <sup>+</sup>CD8<sup>+</sup> T cells in tumors. **(c)**, ELISA analysis of total IgG titers of VSVG in immune sera. **(d)**, Analysis of the expression of VSV-specific neutralizing antibodies in immunized sera using PRNT<sub>50</sub> assay, the dashed line represents the limit of detection. **(e)**, Schematic illustration of the experimental design for evaluating the therapeutic effects of vEVs on the 4T1 model. **(f)**, Individual tumor growth curves recorded every three days. **(g)**, Tumor growth curves. **(h)**, Tumor control rates. **(i)**, Survival curves. **(j-k)**, TUNEL staining **(j)** and Ki67 **(k)** of tumors. ( $n=6$  biologically independent samples)

## Conclusions

In this study, an engineered “self-adjuvant” multiantigenic nanovaccines with LN–tumor dual-targeting was successfully synthesized. Within the LNs, the nanovaccine was efficiently recognized and internalized by DCs, triggering their maturation and provoking a strong immune response against both viral and tumor antigens. Meanwhile, the vEV-mediated homologous tumor targeting and pH-sensitive membrane fusion facilitated the display of viral PAMPs on the tumor cell surface, thereby enhancing the specific recognition and phagocytosis of tumor cells by phagocytes. Consequently, these combined effects confer the nanovaccine with a sustained and potent ability to kill tumor cells. This research offers a versatile and convenient strategy for the development of nanovaccine platforms that are capable of spatiotemporal

immunoregulation and can deliver powerful immunotherapeutic results.

## Abbreviations

ALIX	Apoptosis-Linked Gene-2 Interacting Protein X
ANOVA	Analysis Of Variance
APCS	Antigen-Presenting Cells
B16	Murine Melanoma
BMDCs	Bone Marrow-Derived Dendritic Cells
BMDMs	Bone Marrow-Derived Macrophages
CLSM	Confocal Laser Scanning Microscopy
CPE	Cytopathic Effect
CRT	Calreticulin
CT26	Colorectal Carcinoma
CTL	Cytotoxic T Lymphocyte
DCS	Dendritic Cells
DMEM	Dulbecco'S Modified Eagle Medium
FBS	Fetal Bovine Serum
HEPG2	Human Hepatocellular Carcinoma
ICD	Immunogenic Cell Death
IFN	Type I Interferon
IL-4	Interleukin-4

IL-6	Interleukin-6
LN	Lymph Nodes
MFI	Mean Fluorescence Intensity (
NK	Natural Killer
PBS	Phosphate-Buffered Saline
PRNT	Plaque Reduction Neutralisation Test
TAAS	Tumor-Associated Antigens
TCID <sub>50</sub>	50% Tissue Culture Infectious Dose
tEVs	Tumor Cell-Derived Extracellular Vesicles
TEM	Transmission Electron Microscopy
TLR4	Toll-Like Receptor 4
TNF- $\alpha$	Tumor Necrosis Factor- $\alpha$
TSAS	Tumor-Specific Antigens
vEVs	Virus-Modified Extracellular Vesicles
VERO	African Green Monkey Kidney
VSV	Vesicular Stomatitis Virus
VSVG	Vesicular Stomatitis Virus Glycoprotein
4T1	Mammary Carcinoma

## Supplementary Information

The online version contains supplementary material available at <https://doi.org/10.1186/s12951-025-03208-1>.

Supplementary Material 1

## Acknowledgements

The authors thank the Biological & Medical Engineering Core Facilities (Beijing Institute of Technology) for providing advanced equipment.

## Author contributions

Z. W. and H. C. contributed equally to this study by conducting the majority of the experiments, analyzing the data, and drafting the manuscript. R. M. and W. W. were responsible for developing the mouse models. S. L., Y. J. and Z. Y. assisted with the cell-based experiments. G. L. and L. H. oversaw the experimental design and provided guidance on data analysis and manuscript preparation. All authors have reviewed and approved the final version of the manuscript.

## Funding

This work was funded by the National Natural Science Foundation of China (22274011), Hebei Natural Science Foundation (B2024105013), Beijing Institute of Technology Research Fund Program for Young Scholars (2020–2024), Beijing Natural Science Foundation Proposed Program (L242138).

## Data availability

No datasets were generated or analysed during the current study.

## Declarations

### Ethics approval and consent to participate

All animal experiments were approved by the Experimental Animal Committee of the Beijing Institute of Technology with an approval number: 2019-0010-M-2023152.

### Consent for publication

Not applicable.

### Competing interests

The authors declare no competing interests.

### Author details

<sup>1</sup>School of Medical Technology, Beijing Institute of Technology, Beijing 100081, P. R. China

<sup>2</sup>Center for Child Care and Mental Health (CCCMH), Shenzhen Children's Hospital, Shenzhen 518034, P. R. China

<sup>3</sup>School of Life Sciences, Inner Mongolia Normal University, Hohhot 010022, P. R. China

Received: 8 November 2024 / Accepted: 9 February 2025

Published online: 27 February 2025

## References

1. Fan T, Zhang MN, Yang JX, Zhu ZA, Cao WL, Dong CY. Therapeutic cancer vaccines: advancements, challenges, and prospects. *Signal Transduct Target Therapy*. 2023;8.
2. Katsikis PD, Ishii KJ, Schliehe C. Challenges in developing personalized neoantigen cancer vaccines. *Nat Rev Immunol*. 2024;24:213–27.
3. Evel-Kabler K, Chen SY. Dendritic cell-based tumor vaccines and antigen presentation attenuators. *Mol Ther*. 2006;13:850–8.
4. Liu CP, Wang YC, Li LM, He DY, Chi JX, Li Q, Wu YX, Zhao YX, Zhang SH, Wang L, et al. Engineered extracellular vesicles and their mimetics for cancer immunotherapy. *J Controlled Release*. 2022;349:679–98.
5. Meng FQ, Lin ZD, Ma YM, Che RB, Zhang C, Wei YT, Song X, Liang X, Zhang XD. Engineered algae microrobots as photosynthetic living materials promote T cells' anti-tumor immunity. *Cell Rep Phys Sci*. 2024;5.
6. Li X, Wei Y, Zhang Z, Zhang X. Harnessing genetically engineered cell membrane-derived vesicles as biotherapeutics. *Extracell Vesicles Circulating Nucleic Acids*. 2024;5:44–63.
7. Chen MK, Chen ZX, Cai MP, Chen H, Chen ZF, Zhao SC. Engineered extracellular vesicles: a new approach for targeted therapy of tumors and overcoming drug resistance. *Cancer Commun*. 2024;44:205–25.
8. Wang ZG, Mo HK, He ZY, Chen AM, Cheng P. Extracellular vesicles as an emerging drug delivery system for cancer treatment: current strategies and recent advances. *Biomed Pharmacother*. 2022;153.
9. Yue M, Hu SY, Sun HF, Tuo B, Jia B, Chen C, Wang WK, Liu JB, Liu Y, Sun ZQ, Hu JH. Extracellular vesicles remodel tumor environment for cancer immunotherapy. *Mol Cancer*. 2023;22.
10. Jin SL, Lv ZY, Kang L, Wang JY, Tan CC, Shen LM, Wang L, Liu J. Next generation of neurological therapeutics: native and bioengineered extracellular vesicles derived from stem cells. *Asian J Pharm Sci*. 2022;17:779–97.
11. Jiang Q, Wang L, Tian JL, Zhang WJ, Cui HJ, Gui HL, Zang ZH, Li B, Si X. Food-derived extracellular vesicles: natural nanocarriers for active phytoconstituents in new functional food. *Crit Rev Food Sci Nutr*. 2023.
12. Roerig J, Schulz-Siegmund M. Standardization approaches for extracellular vesicle loading with oligonucleotides and biologics. *Small*. 2023;19.
13. Ghonime MG, Saini U, Kelly MC, Roth JC, Wang PY, Chen CY, Miller K, Hernandez-Aguirre I, Kim Y, Mo XK et al. Eliciting an immune-mediated antitumor response through oncolytic herpes simplex virus-based shared antigen expression in tumors resistant to viroimmunotherapy. *J Immunother Cancer*. 2021;9.
14. Liu GN, Zhu MT, Zhao X, Nie GJ. Nanotechnology-empowered vaccine delivery for enhancing CD8<sup>+</sup> T cells-mediated cellular immunity. *Adv Drug Deliv Rev*. 2021;176.
15. Lichty BD, Power AT, Stojdl DF, Bell JC. Vesicular stomatitis virus: re-inventing the bullet. *Trends Mol Med*. 2004;10:210–6.
16. Zhang YG, Nagalo BM. Immunovirotherapy based on recombinant vesicular stomatitis virus: where are we? *Front Immunol*. 2022;13.
17. Halajian EA, LeBlanc EV, Gee K, Colpitts CC. Activation of TLR4 by viral glycoproteins: a double-edged sword? *Front Microbiol*. 2022;13.
18. Gebremeskel S, Nelson A, Walker B, Oliphant T, Lobert L, Mahoney D, Johnston B. Natural killer T cell immunotherapy combined with oncolytic vesicular stomatitis virus or reovirus treatments differentially increases survival in mouse models of ovarian and breast cancer metastasis. *J Immunother Cancer*. 2021;9.
19. Ghosh S, Kumar M, Santiana M, Mishra A, Zhang M, Labayo H, Chibly AM, Nakamura H, Tanaka T, Henderson W, et al. Enteric viruses replicate in salivary glands and infect through saliva. *Nature*. 2022;607:345.
20. van den Pol AN, Davis JN. Highly attenuated recombinant vesicular stomatitis virus VSV-12'GFP displays immunogenic and oncolytic activity. *J Virol*. 2013;87:1019–34.
21. Shelly S, Lukinova N, Bambina S, Berman A, Cherry S. Autophagy is an essential component of *Drosophila* immunity against vesicular stomatitis virus. *Immunity*. 2009;30:588–98.
22. Huang LL, Wang WW, Wang ZJ, Zhang H, Liu HL, Wu GH, Nie WD, Xie HY. Engineering Oncolytic adenoviruses with VSVG-Decorated tumor cell membranes for synergistically enhanced Antitumor Therapy. *Adv Funct Mater*. 2023;33.
23. Wedge ME, Jennings VA, Crupi MJF, Poutou J, Jamieson T, Pelin A, Pugliese G, de Souza CT, Petryk J, Laight BJ et al. Virally programmed extracellular vesicles

sensitize cancer cells to oncolytic virus and small molecule therapy. *Nat Commun.* 2022;13.

### **Publisher's note**

Springer Nature remains neutral with regard to jurisdictional claims in published maps and institutional affiliations.